Sensors and Actuators B 193 (2014) 428–433

Contents lists available at ScienceDirect

Sensors and Actuators B: Chemical

journal homepage: www.elsevier.com/locate/snb

Conductivity in SnO_2 polycrystalline thick film gas sensors: Tunneling electron transport and oxygen diffusion

C.M. Aldao[a,*], F. Schipani[a], M.A. Ponce[a], E. Joanni[b], F.J. Williams[c]

[a] Institute of Materials Science and Technology (INTEMA), University of Mar del Plata and National Research Council (CONICET), Juan B. Justo 4302, B7608FDQ Mar del Plata, Argentina
[b] CTI Renato Archer, Rodovia D. Pedro I (SP - 65) Km 143.6, CEP: 13069-901 Campinas, SP, Brasil
[c] Departamento de Quimica Inorganica, Analitica y Quimica Fisica and INQUIMAE, Facultad de Ciencias Exactas y Naturales, Universidad de Buenos Aires and CONICET, Pab. 2, piso 3, C1428EHA Buenos Aires, Argentina

ARTICLE INFO

Article history:
Received 28 August 2013
Received in revised form
18 November 2013
Accepted 28 November 2013
Available online 11 December 2013

Keywords:
SnO_2
Electron tunneling
Oxygen diffusion

ABSTRACT

Conduction mechanisms in polycrystalline SnO_2 thick sensing films were investigated by means of DC electrical resistance during heating–cooling cycles. Samples were maintained at relatively high temperatures in H_2 or O_2 ambient atmospheres before performing electrical measurements under vacuum or before performing XPS measurements in order to determine band bending. Results suggest that intergrains present Schottky barriers that are responsible for the observed conductivities regardless of gas pre-treatment. Oxygen diffusion modulates barrier widths affecting conductivity through tunneling transport. The electrical response to subsequent exposure to an oxygen atmosphere is consistent with our interpretation.

1. Introduction

Gas sensors based on semiconducting metal oxides are used to monitor the content of oxidizing and reducing gas molecules in a surrounding medium [1–3]. The goal is the development of low-cost devices, based regularly on gas sensitive materials that change resistance and/or impedance when hazardous substances appear in the ambient. The operational principle of these sensors consists in transforming the adsorption and desorption of different gases into an electrical signal. In particular, gas sensors based on polycrystalline SnO_2 offer some advantages such as low cost, long lifetime, and high selectivity and sensitivity [4–6].

The basic mechanisms responsible for gas sensing in semiconducting metal oxides are generally accepted [1–3]. There is a finite density of electron donors and/or electron acceptors bound to the grain surface of a wide bandgap semiconducting oxide, such as tin oxide. These electron donors or acceptors cause an exchange of electrons with the interior of the semiconducting grains, thus forming a space charge layer close to the surface. By changing the surface concentration and/or the energy distribution of the donors/acceptors, the space charge region is modulated and thus the conductivity. However, despite technological progress, the mechanisms by which intergranular barriers form and electronic conduction occurs are still controversial.

Gas sensor devices consisting of a porous sensing layer of a semiconductor oxide involve gases diffusion in the sensing layer where they are adsorbed on the grain surfaces. Usually, it is assumed that large enough grains present a surface space charge layer and an unaffected bulk. For n-type materials, gases modify the sensor conductivity by altering the amount of negative surface charge associated to acceptor levels at intergrains. With the exposure to reducing (oxidizing) gases, the amount of oxygen ions decreases (increases), the intergrain barriers are reduced (increased), and then conductivity increases (decreases).

In this work we studied the electrical conductance under vacuum of SnO_2 films treated previously in oxygen or hydrogen containing atmospheres as a function of temperature. Furthermore, we determined band bending changes using X-ray photoemission spectroscopy. Subsequently, we also determined the conductivity evolution when films are exposed to an oxygen rich environment. Our results suggest that Schottky barriers are always present and that tunneling transport through barriers is the dominant mechanism controlling conductivity.

2. Experimental

Commercial high-purity SnO_2 (Aldrich, medium particle size 0.4 μm) was ground until a medium particle size of 0.13 μm was

* Corresponding author. Tel.: +54 223 4816600; fax: +54 223 4810046.
E-mail addresses: cmaldao@mdp.edu.ar, cmaldao@fi.mdp.edu.ar (C.M. Aldao).

0925-4005/$ – see front matter © 2013 Elsevier B.V. All rights reserved.
http://dx.doi.org/10.1016/j.snb.2013.11.114

obtained. Then, a paste was prepared with an organic binder (glycerol). The solid/organic binder ratio was ½, and no dopants were added. Thick, porous film samples were prepared by painting onto insulating alumina substrates on which electrodes with an interdigitated shape had been deposited by sputtering as described below. After cleaning the 96% dense alumina substrates with acetone and isopropyl alcohol, they were blown with dry nitrogen and placed in a sputtering chamber. After pumping the chamber to its base pressure (10^{-6} mbar), an adhesion layer consisting of 25 nm of titanium was deposited. Without breaking vacuum, a platinum film 200 nm thick was then deposited over the Ti layer. Both depositions were performed using RF guns with 2-inch targets and 5×10^{-3} mbar, Ar as the working gas. The powers for Ti and Pt depositions were set to 150 W and 100 W, respectively. For defining the electrodes, the substrates with the metal films were placed in a home-built micromachining system consisting of three translation stages and a 20 W, frequency tripled Nd:YVO4 laser (λ = 355 nm). The conditions for removing the platinum film to expose the alumina substrate (thus defining the interdigitated electrodes) were: 0.5 W laser power and 2 mm/s writing speed. The interelectrode distance was 20 μm.

After painting, in order to evaporate the organic binder and to improve the adhesion of films to the alumina substrate, samples were kept at 100 °C for 1 h in air. Later, samples were heated up to 380 °C using a heating rate of 1 °C/min and exposed to dry air at 380 °C during 1 h. Finally, some of the samples were kept at 380 °C for 4 h in a N_2 atmosphere with 5% H_2. Samples were labeled S_{O_2} (samples only exposed to dry air) and S_{H_2} (samples exposed to hydrogen).

The electrical behavior of films was analyzed using a multimeter (Agilent 34401A). Resistance *vs.* temperature measurements for samples S_{O_2} and S_{H_2} were carried out raising and then decreasing the temperature with different temperature ranges at a rate of ~2 °C/min with the samples kept in vacuum (≈10^{-4} mbar). Later, the resistance of the film labeled S_{H_2} was measured while raising and then decreasing the temperature from room temperature up to 380 °C at a rate of ~2 °C/min with the sample kept in a dry air atmosphere (atmospheric pressure).

X-ray Photoelectron Spectroscopy measurements (XPS) were performed under UHV conditions (base pressure < 5×10^{-10} mbar) in a SPECS spectrometer system equipped with a 150 mm mean radius hemispherical electron energy analyzer and a nine channeltron detector. XPS spectra were acquired at a constant pass energy of 20 eV using an un-monochromated Mg *K*α (1253.6 eV) source operated at 12.5 kV and 20 mA and a detection angle of 30° with respect to the sample normal on grounded conducting substrates. The binding energies quoted are referred to the Au $4f_{7/2}$ emission at 84.0 eV.

3. Conduction mechanisms

Tin dioxide is a wide gap n-type semiconductor with a band gap of about 3.6 eV. Although different types of defects are present in SnO_2, oxygen vacancies, which behave as electron donors, are dominant. It has long been recognized that the resistance of this type of gas sensors is determined by Schottky barriers at grain surfaces [4]. Therefore, the key issues are barrier formation at intergrains and electron transport between grains. Adsorption of different gases is accompanied by changes in barriers heights. This in turn affects electron transport between grains and thus the resistance of the device changes. Conduction mechanisms have been interpreted in analogy to those in metal-semiconductor contact diodes. Accordingly, the electrical properties of polycrystalline semiconductors are usually described with a simple one-dimensional model representing the interface between two grains. Fig. 1 depicts the double Schottky barrier model that is generally accepted. In spite of possible complexities due to the randomness of the structure, usually a so-called bricklayer model with cubic-shaped grains of identical size is assumed [7]. Also, it is regularly considered that a thermionic mechanism is responsible for the sample conductivity. This conduction mechanism is described by [8]

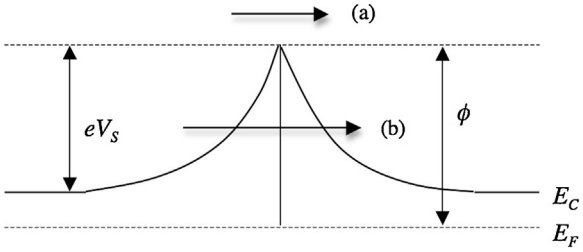

Fig. 1. Diagram for the intergranular double-Schottky barrier model. The band bending is eV_S and ϕ the height of the barrier. Arrow (a) indicates emission of electrons from the left grain to the right grain over the top of the barrier, the thermionic contribution to current transport. Arrow (b) indicates quantum mechanical tunneling through the barrier, the thermionic-field emission contribution to electron transport.

$$G = G_0 \exp(-eV_S/kT) \quad (1)$$

where V_s is the band bending, T the temperature, and k the Boltzmann constant. This equation reflects an activated process due to intergranular barriers. Using Eq. (1) (*i.e.* assuming an Arrhenius relation) the band bending, or the barrier height ϕ that can be defined as the band bending or $eV_S + E_C - E_F$ (as shown in Fig. 1), is regularly estimated. Indeed, by plotting the conductance (ln G) *vs.* the reverse function of temperature ($1/T$), an activation energy can be obtained [9].

It has been pointed out that a thermionic-field emission or tunneling contributions are unavoidable for the usual barriers characteristics [10]. The tunneling current can be calculated with

$$J_{\text{tunneling}} = \frac{AT}{k} \int_0^{eV_s} F(E)P(E)dE \quad (2)$$

where $F(E)$ is the Fermi–Dirac distribution and $P(E)$ is the transmission probability, which can be determined by means of the Wentzel–Kramer–Brillouin (WKB) approximation [11]. Despite its relevance most researchers do not include this contribution in their calculations [6]. Indeed, typical proposed band bendings and dopant concentrations make thermionic-field emission the most relevant conduction mechanism in many cases.

As discussed above, two models have been used in the literature to rationalize electron conduction in polycrystalline SnO_2: (i) an activated thermionic mechanism that depends only on intergranular barrier heights and (ii) an electron tunneling mechanism that depends both on intergranular barrier heights and widths. As we should see below temperature dependence conductance measurements as well as band bending measurements can be used jointly to discriminate the dominant electron conduction mechanism.

4. Results and discussions

Before presenting the polycrystalline SnO_2 conductance measurements, it is important to determine the chemical composition of the samples employed, as the presence of undesirable contaminants could have dramatic effects on conductivity. Therefore, we have characterized our samples with X-ray photoemission spectroscopy (XPS). Fig. 2 shows XPS spectra corresponding to the oxygen annealed SnO_2 sample (S_{O_2}) and the oxygen annealed followed by hydrogen reduction SnO_2 sample (S_{H_2}). Broad scans show the presence of only Sn and O related peaks with no detectable amounts of undesirable contaminants. The later corroborates the

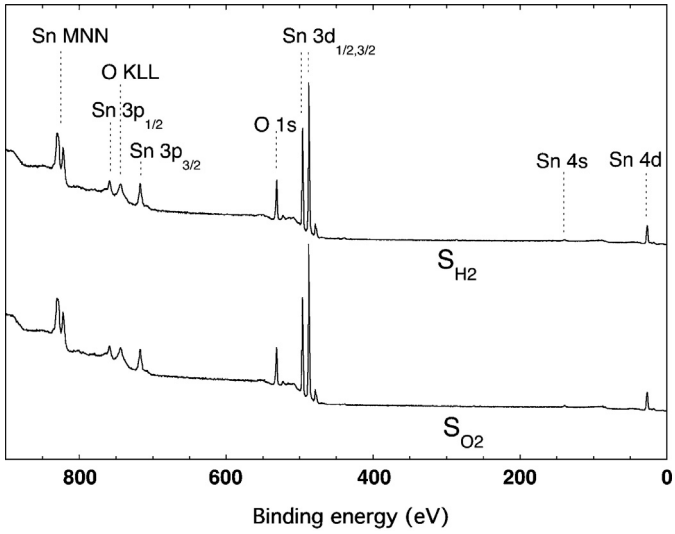

Fig. 2. S_{O_2} and S_{H_2} XPS broad scans. Only Sn and O related XPS peaks are observed indicating the absence of contaminants in detectable amounts.

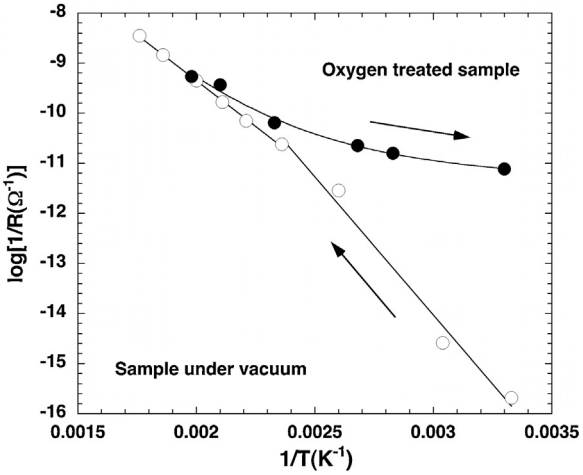

Fig. 4. Conductance cycle for the S_{O_2} sample under vacuum up to 295 °C. After cooling down, the conductivity adopts a much larger value than at the beginning of the cycle. Lines are a guide to the eye.

absence of possible impurities on the semiconductor surface. Furthermore, note the complete absence of C 1s signals expected at approximately 285 eV in both cases. This is a significant finding as it indicates that the oxygen treatment employed was successful in removing the organic binder employed during sample preparation. Therefore, these data indicate that, within the sensitivity of our XPS measurements, we are dealing with well-defined samples, an important point in conductivity measurements.

Fig. 3 shows the conductance under vacuum of oxygen treated (S_{O_2}) and hydrogen treated (S_{H_2}) samples *vs.*the inverse of temperature, in cycling experiments. Specifically, conductance was measured by raising and then decreasing the temperature under vacuum reaching about 140 °C. In this temperature range, the conductivity change for the S_{H_2} sample is quite small (slope of 0.17 eV) and the room temperature value is recovered after the cycle. The S_{O_2} sample shows a conductance change that corresponds to an average activation energy of 0.45 eV. Furthermore, the room temperature conductance increases about 50% after reaching the highest temperature.

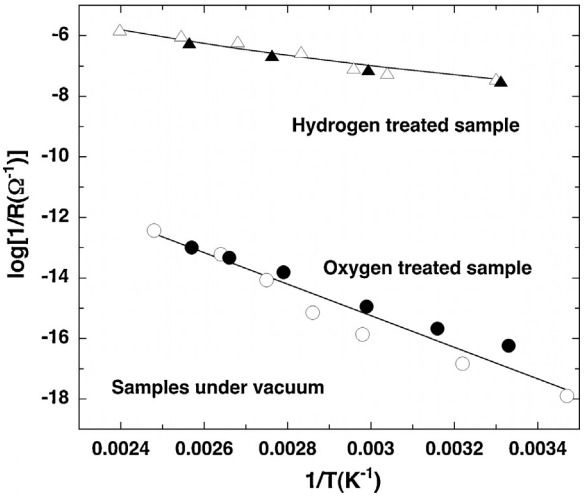

Fig. 3. Conductance for the hydrogen (S_{H_2}) and oxygen (S_{O_2}) treated samples in temperature cycling experiments up to 140 °C. The line for the sample S_{H_2} corresponds to the conductivity of a Schottky diode with a barrier height of 0.69 eV and dopant concentrations of 1.8×10^{19} cm^{-3}. The line for the sample S_{O_2} is just a guide to the eye.

Fig. 4 also shows a temperature cycle for the S_{O_2} sample under vacuum; in this case, the temperature was raised up to 295 °C, a typical temperature used in gas detection with this type of sensors. As expected, the conductance presents the same behavior as shown in Fig. 3 during heating up to 150 °C with a 0.45 eV activation energy. Note however that a further increase in temperature results in an activation energy decrease to 0.31 eV. Finally when the cycle is reversed and the temperature is decreased, the conductivity presents higher values, reaching a room temperature value two order of magnitude greater than the initial one. Conversely, a similar cycle for the S_{H_2} (not shown) presents a similar behavior to that of Fig. 3, and the room temperature value is recovered at the end of cycle.

Let us first interpret the results of Fig. 3 using the thermionic model based on Eq. (1) and neglecting electron tunneling. The S_{H_2} sample conductivity was high due to a low intergrain oxygen amount that is not affected by the heat treatment; *i.e.*, the oxygen amount at the intergrains remains constant during the temperature cycle. Different conductivities between the S_{H_2} and the S_{O_2} samples would indicate barriers about 0.3 eV lower for the hydrogen treated samples, consistent with the observed slopes.

In contrast to Fig. 3, the results of Fig. 4 are not easy to explain within the frame of a thermionic mechanism for conduction. With heating, the conductivity increases with a slope corresponding to an activation energy of 0.45 eV. Interestingly, above 150 °C, the slope reduces to 0.31 eV indicating that the activation energy, according to Eq. 1, must change in the 150–295 °C range. First, we can assume that oxygen desorbs as the temperature is increased and then the activation energy would decrease with *T*. However, with a reducing barrier height, the conductivity should increase faster than at low temperatures, as a low activation energy facilitates conduction. Second, we can assume that the activation energy increases with *T*. This could be due to the adsorbed oxygen that is in the form of O_2^- below 150 °C while above this temperature it chemisorbs as O^- or O^{2-} [12]. However, after cooling down, the conductivity adopts a much larger value than at the beginning of the cycle, result that is incompatible with a higher barrier.

As discussed above the activated thermionic model described by equation 1 fails to interpret the data presented in Fig. 4. A different reason for this type of behavior can be put forward. When heating the samples to a high enough temperature, oxygen intragranular diffusion takes place [13,14]. This phenomenon affects the oxygen vacancies concentration and then the width

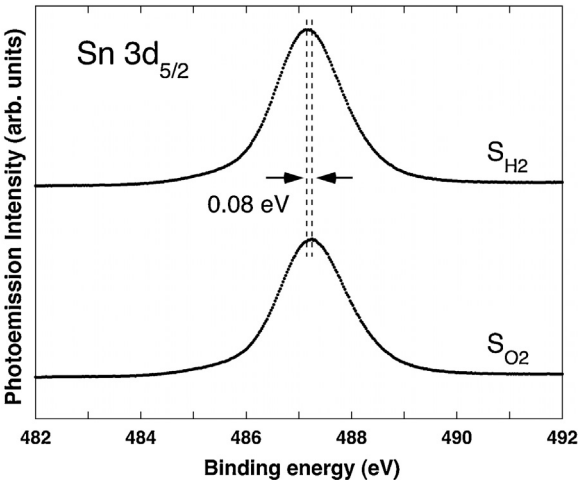

Fig. 5. Sn 3d5/2 core level energy distribution curves for the S_{H_2} and the S_{O_2} samples. Similar binding energy indicates that barrier heights do not differ considerably.

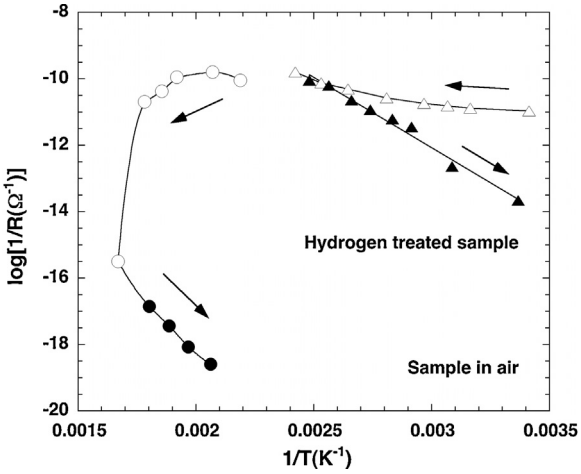

Fig. 6. Conductance cycles for the S_{H_2} sample in air up to 140 °C and 325 °C. After the second cycle, the conductivity reduces abruptly. Lines are a guide to the eye.

of the intergranular potential barriers. The thermionic contribution to conductivity would not be modified as long as the band bending remains constant, see Eq. (1). Conversely, the thermionic-field emission contribution would be strongly altered as tunneling depends on both height and width of the barriers, Eq. (2).

If tunneling contribution to conductivity is relevant, the results of Fig. 3 can be interpreted as follows. The S_{H_2} sample is expected to have a high density of oxygen vacancies and then narrow barriers that facilitate tunneling. Thus, the high conductivity and its small temperature dependence would be a direct effect of tunneling through a narrow barrier. The S_{O_2} sample is expected to have a lower density of oxygen vacancies and then wider barriers. Consequently, its conductivity is expected to be much lower than for the S_{H_2} sample and its dependence with temperature higher, as observed.

Results of Fig. 4 have also a direct interpretation if tunneling is the dominant mechanism in conduction. Indeed, as temperature is raised, oxygen can diffuse out of the S_{O_2} sample increasing the donor density. Thus, tunneling is favored and after cooling down the sample presents a much higher conductivity. In a low doped sample, grains can be completed depleted. As doping increases, grains can have a bulk region in their centers. The slope change in conductivity at about 140 °C is an indication that oxygen diffusion led to a doping that narrowed the space charge regions to the point at which grains were not completed depleted [15–17].

By means of XPS core level analysis, comparative values of the interface Fermi level position in the gap can be determined as it is directly related to the XPS peak binding energy position. In particular, the Sn3d5/2 peak can be used due to the quality of the signal that can be obtained as presented in Fig. 5 [18,19]. Results obtained for the S_{H_2} and the S_{O_2} samples show that barrier heights do not differ considerably. Interestingly, the barrier for the S_{H_2} sample is slightly higher than that for the S_{O_2} sample. Fittings indicated a difference in binding energy of 0.08 eV, as shown in Fig. 5. Therefore, the Schottky barrier height for the S_{H_2} sample is 0.08 eV higher than for the S_{O_2} sample.

We determined the binding energy from other core levels of Sn, specifically Sn4d and Sn4s, and also from O 1s. Results confirmed a Schottky barrier difference of 0.06 ± 0.04 eV with a slightly higher barrier for the S_{H_2} sample. These results represents strong evidence in favor of a dominant tunneling conduction mechanism as the thermionic contribution only depends on Schottky barrier height and then it could not be responsible for the conductivity experimentally observed.

Finally, we heated up the sample S_{H_2} in air as shown in Fig. 6. The exposure to air at room temperature very rapidly leads to a reduction in conductivity. Then, conductance was measured by raising and then decreasing the temperature reaching about 140 °C. After the cycle, the resistance increased from 58 KΩ to 860 KΩ, indicating doping changes since quite low temperatures. By heating up to 325 °C, the conductivity suddenly drops and the resistance becomes higher than 5 MΩ. With the subsequent cooling of the sample, the resistance increases very fast to values higher than 100 MΩ, which is beyond our detection. These findings are consistent with the action of two mechanisms. At room temperature, barrier heights increase due to the presence of oxygen and then the conductivity reduces. Heating up to 140 °C affects the conductivity moderately but for higher temperatures the conductivity reduces abruptly. We attribute this large change to a lower vacancy density due to oxygen diffusion into the grains, which directly affects tunneling contribution to conduction.

So far we have argued qualitatively in favor of a tunneling conduction mechanism in order to interpret our data. Let us now fit our findings including tunneling contributions to conductivity as expressed in Eq. (2). As mentioned, a double Schottky barrier model is widely accepted to describe polycrystalline semiconductor intergrains. However, many researchers consider grain boundaries of essentially zero width, while others take into account a non-negligible disordered layer at the grain boundaries, such that the electron transport occurs in two steps [10]. Since the main conclusions will not differ, for the sake of simplicity we adopted here the second assumption. Also, we will assume that barriers are spatially uniform to allow a one-dimensional treatment [20].

The interpretation of conductivity in nanocrystalline semiconductors, normally acknowledged in the field of gas sensing, is inaccurate as it neglects tunneling contribution. Transport analysis requires calculating the probability that an electron can pass from one side of the potential barrier to the other. We can resort to the WKB approximation

$$P(E) = \exp\left[-2\int_{x_1}^{x_2} \alpha(x)dx\right] \tag{3}$$

where the limits x_1 and x_2 are the classical turning points and

$$\alpha(x) = \frac{\sqrt{2m}}{\hbar}[V(x) - E]^{1/2} \tag{4}$$

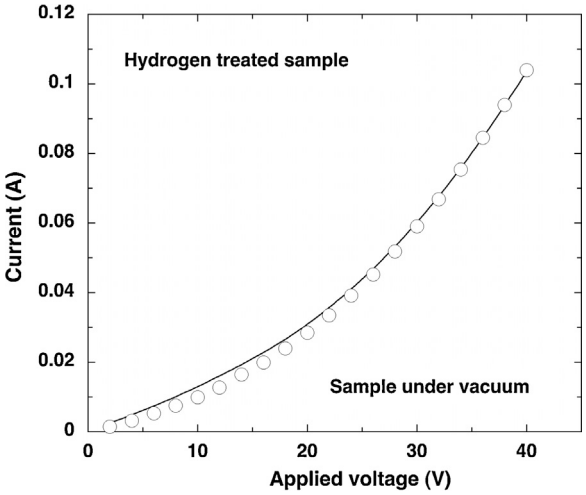

Fig. 7. Current–voltage curve for the sample S_{H_2} under vacuum. The non-linear characteristic indicates the presence of intergrain barriers. The line corresponds to the *I–V* characteristic of a Schottky diode in reverse with the determined barrier height from Fig. 2 (0.69 eV) and donor concentration ($N_d = 1.8 \times 10^{19}\,cm^{-3}$).

After integrating Eq. (3), the probability for an electron to pass the barrier is

$$T = \exp\left\{-\frac{(eV_s)^{1/2}A\sqrt{2m}}{\hbar}\left[\left(1-\frac{E}{eV_s}\right)^{1/2} - \frac{E}{eV_s}\log\left(\frac{1+\left(1-\frac{E}{eV_s}\right)^{1/2}}{\left(\frac{E}{eV_s}\right)^{1/2}}\right)\right]\right\} \quad (5)$$

Now, Eq. (2) can be applied using any regular computing method. According to the geometry of our sensors, the electrical resistance can be related to that of semi-infinite electrodes, coplanar with a gap separating them. Thus, the corresponding resistivity can be determined from resistance measurements [21].

Fig. 3 includes results of our fittings using Eqs. (2) and (5) for the sample S_{H_2}. A high doping is expected as result of the thermal treatment under a hydrogen containing atmosphere. Indeed, the filled line represents the expected conductivity values for a dopant concentration $N_d = 1.8 \times 10^{19}\,cm^{-3}$ and a band bending $eV_s = 0.69$ eV, values that are consistent with capacitance measurements (not reported here).

It is interesting to note that the barrier height is not as low as one could expect after a treatment in a reducing atmosphere. It seems that the effect of this treatment reflects on the high doping that we understand are oxygen vacancies. It is also important to note that the system is quite complicated as grains with different sizes form a complex structure and intergranular barriers are not necessarily uniform nor parabolic [22]. Therefore, we expect far from negligible errors in applying the simple model presented here. However, we showed that tunneling transport happens to be a conduction mechanism that can explain the dominant observations.

As discussed above, the S_{O_2} sample, previous to the thermal cycle, has grains depleted of carriers. Thus, its doping must be lower than $7 \times 10^{17}\,cm^{-3}$ assuming grains with a diameter of about 130 nm. After the temperature cycling, based on the resulting conductivity, our calculations indicate that doping increased to $8 \times 10^{18}\,cm^{-3}$.

The exposure of the sample S_{H_2} to vacuum, and especially after a treatment in a reducing atmosphere, could provoke the absence of negative surface charge associated to oxygen, responsible for surface acceptor levels. However, we have seen that the high observed conductivity can be the consequence of narrow intergranular Schottky barriers due to high donor concentrations.

If there were no intergrains barriers, for a flat band condition or in the presence of accumulation layers, the sample would have an ohmic behavior (linear and symmetric). In Fig. 7 we present the current-voltage curve for the sample S_{H_2} under vacuum that is clearly non linear, far from ohmic. The line corresponds to the I–V characteristic of a Schottky diode in reverse with the determined barrier height from Fig. 2 (0.69 eV) and donor concentration ($N_d = 1.8 \times 10^{19}\,cm^{-3}$). We considered that all the applied voltage drops in the inverse biased diode, approximation that overestimates the conductivity. Anyway, the result is surprisingly good, given the number of simplifications we have adopted. The important point is that tunneling through a narrow barrier presents the electrical behavior observed experimentally, with the nonlinear behavior typical for a diode.

5. Conclusions

We have presented a series of experiments that would be very difficult to explain by considering that conductivity in polycrystalline SnO_2 depends only on intergranular barrier heights. Interestingly, XPS results show that samples with different conductivities can present similar barrier heights. Thus, a thermionic mechanism cannot be responsible for the observed differences. It is expected that the preparation of the samples before measurements lead to samples with different vacancy density and then with different intergranular barrier widths. Thus, the observed results come naturally with the incorporation of tunneling contributions to conductivity as barrier widths directly affect this conduction mechanism.

Acknowledgments

This work was partially supported by the National Council for Scientific and Technical Research (CONICET) of Argentina and the National University of Mar del Plata (Argentina).

References

[1] M.J. Madou, R. Morrison, Chemical Sensing with Solid State Devices, John Wiley & Sons, Inc, New York, NY, 1989.
[2] N. Yamazoe, Toward innovations of gas sensor technology, Sensors and Actuators B: Chemical 108 (2005) 2–14.
[3] N. Barsan, D. Koziej, U. Weimar, Metal oxide-based gas sensor research: how to? Sensors and Actuators B: Chemical 121 (2007) 18–35.
[4] W. Gopel, K. Schierbaum, SnO_2 sensors: currents status and future prospect, Sensors and Actuators B: Chemical 26 (1995) 1–12.
[5] C. Malagù, M.C. Carotta, H. Fissan, V. Guidi, M.K. Kennedy, F.E. Kruis, G. Martinelli, T.G.G. Maffeis, G.T. Owen, S.P. Wilks, Surface state density decrease in nanostructured polycrystalline SnO_2: modelling and experimental evidence, Sensors and Actuators B: Chemical 100 (2004) 283–286.
[6] N. Barsan, U. Weimar, Conduction model of metal oxide gas sensors, Journal of Electroceramics 7 (2001) 143–167.
[7] J. Fleig, The grain boundary impedance of random microstructures: numerical simulations and implications for the analysis of experimental data, Solid State Ionics 150 (2002) 181–193.
[8] N. Barsan, M. Hübner, U. Weimar, Conduction mechanisms in SnO_2 based polycrystalline thick film gas sensors exposed to CO and H_2 in different oxygen backgrounds, Sensors and Actuators B: Chemical 157 (2011) 510–517.
[9] F. Schipani, C.M. Aldao, M.A. Ponce, Schottky barriers measurements through Arrhenius plots in gas sensors based on semiconductor films, AIP Advances 2 (2012) 2158–3226.
[10] M.S. Castro, C.M. Aldao, Prebreakdown conduction in zinc oxide varistors: thermionic or tunnel currents and one-step or two-step conduction processes, Applied Physics Letters 63 (1993) 1077–1079.
[11] C.R. Crowell, V.L. Rideout, Normalized thermionic-field (T-F) emission in metal-semiconductor (Schottky) barriers, Solid-State Electronics 12 (1969) 89–105.
[12] M. Batzill, U. Diebold, The surface and materials science of tin oxide, Progress in Surface Science 79 (2005) 47–154.
[13] B. Kamp, R. Merkle, J. Maier, Chemical diffusion of oxygen in tin dioxide, Sensors and Actuators B: Chemical 77 (2001) 534–542.

[14] G. Blaustein, M.S. Castro, C.M. Aldao, Influence of frozen distributions of oxygen vacancies on tin oxide conductance, Sensors and Actuators B: Chemical 55 (1999) 33–37.
[15] M.A. Ponce, M.S. Castro, C.M. Aldao, Influence of oxygen adsorption and diffusion on the overlapping of intergranular potential barriers in SnO_2 thick-films, Materials Science and Engineering B 111 (2004) 14–19.
[16] C.M. Aldao, D.A. Mirabella, M.A. Ponce, A. Giberti, C. Malagù, Role of intra-grain oxygen diffusion in polycrystalline tin oxide conductivity, Journal of Applied Physics 109 (2011) 063723.
[17] C. Malagù, A. Giberti, S. Morandi, C.M. Aldao, Electrical and spectroscopic analysis in nanostructured SnO2: long term resistance drift is due to in-diffusion, Journal of Applied Physics 110 (2011) 093711.
[18] T.G.G. Maffeis, G.T. Owen, M.W. Penny, T.K.H. Starke, S.A. Clark, H. Ferkel, S.P. Wilks, Nano-crystalline SnO_2 gas sensor response to O_2 and CH_4 at elevated temperature investigated by XPS, Surface Science 520 (2002) 29–34.
[19] M. Kwoka, L. Ottaviano, J. Szuber, Photoemission studies of the surface electronic properties of L-CVD SnO_2 ultra thin films, Applied Surface Science 258 (2012) 8425–8429.
[20] Y. Kajijawa, Conduction model covering non-degenerate through degenerate polycrystalline semiconductors with non-uniform grain-boundary potential heights based on an energy filtering model, Journal of Applied Physics 112 (2012) 123713.
[21] C. Belmont, H.H. Gtrault, Coplanar interdigitated band electrodes for synthesis Part I: Ohmic loss evaluation, Journal of Applied Electrochemistry 24 (1994) 475–480.
[22] W. Izydorczyk, Numerical analysis of an influence of oxygen adsorption at a SnO_2 surface on the electronic parameters of the induced depletion layer, Physica Status Solidi B Basic Solid State Physics 248 (2011) 694–699.

Biographies

Celso M. Aldao completed his Ph.D. at the Department of Chemical Engineering and Materials Science of the University of Minnesota in 1989. He was appointed as Professor in 1989 at the University of Mar del Plata. Since 1992 he is a member of the research staff of the National Research Council (CONICET). His research activities focus on the physics and chemistry of surfaces and interfaces, with special emphasis on semiconductors.

Federico Schipani obtained his B.Sc. in Physics in 2012 in the University of Mar del Plata. At the moment is a Ph.D. student in the same university. His main interests are gas sensing properties and conduction mechanism in polycristalline semiconductors.

Miguel A. Ponce obtained his B.Sc. in Chemistry in 1999 and PhD in Material Science in 2005 from Mar del Plata National University, Argentina. Since April 2007 he is a member of the research staff of the National Research Council (CONICET). His current research interest includes the development of electronic conduction mechanism of functional inorganic materials.

Ednan Joanni has a Ph.D. degree from the University of Sheffield (1990). He is currently a researcher at CTI (Renato Atcher) Campinas, Brazil. His main interests are in thin film deposition by physical methods, nanostructures, semiconducting oxides, dielectrics, sensors and memories.

Federico J. Williams completed his Ph.D. at the University of Cambridge in 2000. He is currently professor at the University of Buenos Aires and member of the research staff of the National Research Council (CONICET). His current research interests are in the surface chemistry of electroactive self-assembled monolayers.